Bio-Inspired Carbon Nanotube–Polymer Composite Yarns with Hydrogen Bond-Mediated Lateral Interactions

Allison M. Beese,[†] Sourangsu Sarkar,[‡] Arun Nair,[§] Mohammad Naraghi,[†,∥] Zhi An,[‡] Alexander Moravsky,[⊥] Raouf O. Loutfy,[⊥] Markus J. Buehler,[§,*] SonBinh T. Nguyen,[‡,*] and Horacio D. Espinosa[†,*]

[†]Department of Mechanical Engineering, Northwestern University, 2145 Sheridan Road, Evanston, Illinois 60208-3111, United States, [‡]Department of Chemistry, Northwestern University, 2145 Sheridan Road, Evanston, Illinois 60208, United States, [§]Department of Civil and Environmental Engineering, Massachusetts Institute of Technology, 77 Massachusetts Avenue, Cambridge, Massachusetts 02139, United States, and [⊥]MER Corporation, 7960 South Kolb Road, Tucson, Arizona 85706, United States. [∥]Present address: M.N.: Department of Aerospace Engineering, Texas A & M University, 3141 TAMU, College Station, TX 77843-3141 (USA).

ABSTRACT Polymer composite yarns containing a high loading of double-walled carbon nanotubes (DWNTs) have been developed in which the inherent acrylate-based organic coating on the surface of the DWNT bundles interacts strongly with poly(vinyl alcohol) (PVA) through an extensive hydrogen-bond network. This design takes advantage of a toughening mechanism seen in spider silk and collagen, which contain an abundance of hydrogen bonds that can break and reform, allowing for large deformation while maintaining structural stability. Similar to that observed in natural materials, unfolding of the polymeric matrix at large deformations increases ductility without sacrificing stiffness. As the PVA content in the composite increases, the stiffness and energy to failure of the composite also increases up to an optimal point, beyond which mechanical performance in tension decreases. Molecular dynamics (MD) simulations confirm this trend, showing the dominance of nonproductive hydrogen bonding between PVA molecules at high PVA contents, which lubricates the interface between DWNTs.

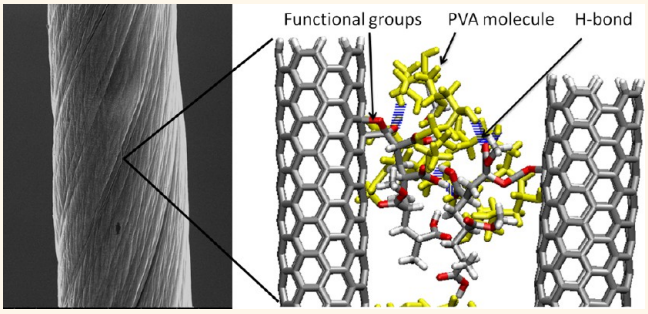

KEYWORDS: carbon nanotube · yarn · polymer composite · hydrogen-bonding · bio-inspired · molecular dynamics

As carbon nanotubes (CNTs) are known to possess high strength and toughness,[1,2] high thermal stability,[3,4] and good electrical conductivity,[5] their use as building blocks in multifunctional nanocomposites, especially those incorporating polymers, has been the subject of extensive research.[6−23] Several strategies have been utilized to disperse CNTs into various polymeric matrices, including solution mixing,[12,13,15,24,25] soaking of CNT buckypaper in polymer solution,[6] *in situ* polymerization,[11,14,17,18] and melt blending.[10] In most of these cases, the CNT content in the composites is relatively low (<20 wt %), which results in lower thermal and electrical conductivity, lower thermal stability, and considerably inferior mechanical properties of the nanocomposite compared to those of CNTs themselves.[10,24,26−29] To incorporate higher volume fractions of CNTs into polymer-based fibers and achieve better mechanical properties, a broad range of fabrication approaches have been taken by researchers, including spinning from CNT solution, spinning from CNT arrays, spinning from CNT aerogel, and twisting or rolling of CNT films, as summarized in a recent review article.[30]

To integrate the remarkable nanoscale properties of CNTs into macroscopic composites, several challenges must be overcome, including achieving a high degree of CNT alignment, optimizing the interactions between neighboring CNTs, and maximizing the interactions between the CNTs and the polymer matrices.[31] Regarding these interactions, several strategies have been

* Address correspondence to espinosa@northwestern.edu, stn@northwestern.edu, mbuehler@mit.edu.

Received for review January 22, 2013 and accepted March 22, 2013.

Published online April 02, 2013
10.1021/nn400346r

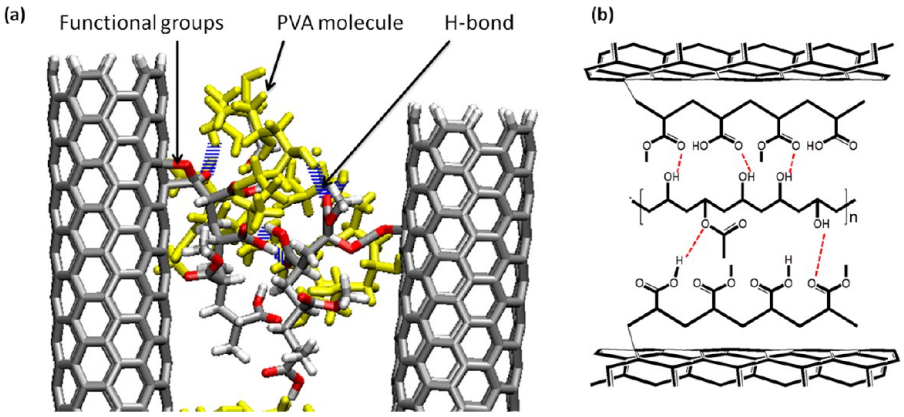

Figure 1. Schematics of hydrogen-bond interactions between the intrinsic organic coating containing carboxylic acid and ester functionalities and the polymer (PVA) containing donor−acceptor hydroxyl groups. The hydrogen bonds and the covalent bonds are shown by broken and solid lines, respectively, in the 3-dimensional Visual Molecular Dynamics (VMD) representation and the 2-dimensional ChemDraw representation.

explored, including chemical functionalization of the relatively inactive CNTs surfaces,[14,24,32−34] which allows them to more efficiently bind to the adjacent CNTs or the surrounding polymer matrix and enhances the strength and toughness of the CNT−CNT or CNT−matrix interactions. However, this chemical functionalization frequently introduces sp^3 defects, which disrupt $\pi - \pi$ conjugation, and thus decrease the inherent mechanical properties, thermal stability, and electrical conductivity of the CNTs.[24,26] Therefore, it is desirable to develop procedures through which high-quality CNTs can be functionalized without disrupting the structural integrity of the CNTs.

In this work, the load transfer mechanisms of natural materials, such as collagen and spider silk[35] have been closely reproduced in CNT−PVA (PVA, poly(vinyl alcohol)) composite yarns. In spider silk, an extensive network of hydrogen bonds and flexible proteins link stiff, "nanocrystalline" protein domains, and as the material deforms, the hydrogen bonds break and reform, allowing for the unfolding of the flexible protein regions.[36−39] In the CNT−PVA yarns described here, we utilize CVD-grown high-quality double-walled carbon nanotube (DWNT) bundles—inherently functionalized during the CVD growth with short polymer chains possessing carboxylic acid and ester functional groups and having only very minor structural defects (Raman D:G peak of ~0.025)[31]—and PVA molecules as the building blocks. The novelty of this study lies in the full characterization and subsequent utilization of the inherent polymer coating, which is strongly attached to the DWNT bundles as previously reported by our group.[31] Through hydrogen bonding to this inherent coating, the flexible PVA chains link the adjacent stiff DWNT bundles, providing a structure that is functionally similar to spider silk and collagen. By varying the ratio of PVA to CNTs, we can alter the density of hydrogen bonds and affect the macroscopic mechanical properties, thus identifying an optimal ratio DWNT/PVA for the best mechanical performance. We also study the nanoscale deformation mechanisms through Molecular Dynamics (MD) simulations, and confirm the parabolic trend in stiffness *versus* PVA content.

RESULTS AND DISCUSSION

Double Wall Nanotube (DWNT) Bundles. The CNT−PVA yarns presented are composed mainly of the DWNT bundles linked by chains of PVA. The DWNT bundles, fabricated by MER Corp. as highly porous mats, approximately 10 μm thick and 30 cm × 30 cm, of disordered bundles, are formed in a chemical vapor deposition (CVD) process using a floating catalyst system with ferrocene as the catalyst precursor and ethyl alcohol as the hydrocarbon feedstock. Each bundle contains several tens of DWNTs, resulting in bundles that are a few tens of nanometers in diameter.[31] In addition to DWNT bundles, the mats contain ~20 wt % catalyst particles, ~5 wt % amorphous carbon, and ~1 wt % graphitic carbon shells surrounding the catalyst particles, and ~15 wt % organic coating, referred herein as the *inherent polymer coating*, as determined by thermogravimetric analysis (TGA)[31] and X-ray photoelectron spectroscopy (XPS).[40] This polymer coating completely covers the DWNT bundles. As fabricated, this inherent polymer coating is primarily a combination of oligomeric chains consisting of ~10 monomeric units of substituted acrylic acids and esters with the general formula of RCH═CR′COOR″, where the R, R′, and R″ groups are hydrogen, alkyl, alkenyl, and aryl groups in various combinations, as described in our previous work.[31] Three-dimensional and two-dimensional schematics of the polymeric coating elucidated from the above analyses are given in Figure 1.

The previously reported C1s XPS spectrum of the DWNT mat[40] reveals the presence of the aforementioned oxygen-containing moieties on the nanotube

surface. Analysis of the full XPS spectrum reveals a carbon-to-oxygen (C/O) ratio of ~10, suggesting good coverage of oxygen-containing moieties on the nanotube surface, which would enhance the interaction between as-synthesized DWNTs and a hydrogen-bonding capable polymer matrix such as PVA.

While an appreciable amount (~15 wt %) of the inherent polymer coating materials can be extracted from the DWNT bundles by sonication in organic solvents such as acetone and methyl ethyl ketone, and ~50 wt % by prolonged Soxhlet extraction in these same solvents, the majority of the inherent organic coating remains firmly attached to the surface of the CNT bundles, most likely through covalent bonds (see Materials and Methods section). The IR spectra of the DWNT bundles heat-treated at 400–600 °C in inert atmosphere for as long as 1 h still show the presence vibration bands of the C–H and C═O groups belonging to the intrinsic polymer, consistent with the covalent bonding of the coating to the nanotube walls.[40] The ^{1}H NMR spectrum of the extracted coating in acetone-d_6 (Figure 2a) shows characteristic resonances for carboxylic acid and ester groups at 11.3 and 2.3 ppm, respectively, as well as those likely associated with polymer backbone (multiple peaks at 0.8–1.6 ppm). The ^{13}C NMR spectrum (Figure 2b) additionally confirms the presence of such polymeric structures. It is interesting to note that the presence of the inherent polymer coating attached to the DWNTs does not lead to significant disruption of the sp^2 C–C bonds of the DWNTs; instead, the intensity ratio between D and G bands (I_D/I_G) from a Raman spectrum of the as-synthesized DWNTs is only ~0.025, indicating that they have minimal defects.[31] This low level of defects is further confirmed by the C1s XPS spectrum,[40] where only a weak peak corresponding to defects[41] can be resolved at 285.5 eV. The high-quality structure of these CVD-in situ-functionalized DWNTs is in stark contrast to the highly defective structures for CNTs made by other postsynthesis functionalization strategies, such as acid and ozone treatments.[24,26,32]

DWNT–PVA Yarn Fabrication. A spinning system was designed and used in the fabrication of DWNT–PVA yarns (Figure 3). The manufacturing process consists of twisting and stretching ribbons cut from CVD-grown DWNT mats (see Materials and Methods section for details). PVA impregnation is achieved by spraying a solution of PVA (0.01–5.0 wt %) in dimethyl sulfoxide (DMSO) on the DWNT ribbons during the spinning process. DMSO was chosen as the solvent as it wets the hydrophobic DWNTs better than water, thus improving PVA infiltration between DWNT bundles.[42] The selection of PVA was inspired by natural materials such as bone, collagen, and spider silk, where high ductility and energy dissipation during deformation is achieved through an extensive hydrogen-bond network: the applied load is transferred between hard and soft

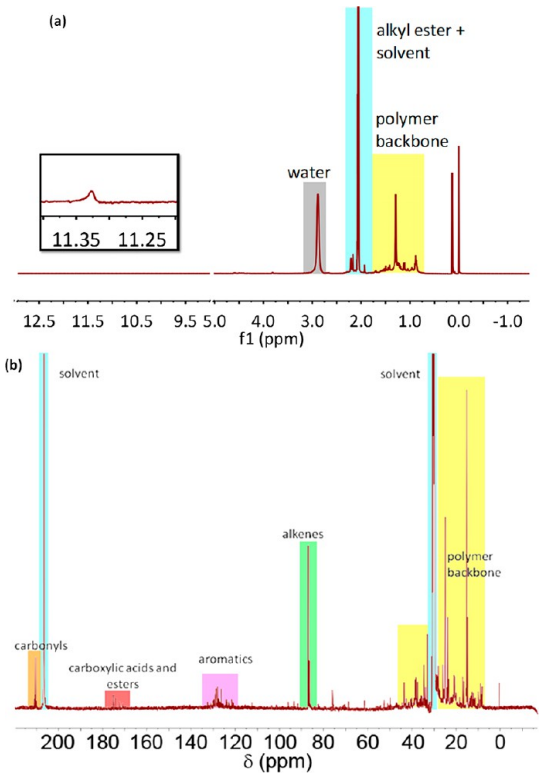

Figure 2. Chemical analysis by (a) ^{1}H NMR, and(b) ^{13}C NMR, which show the presence of a mixture of carboxylic acids and esters in the *inherent organic coating*.

nanoscale components by an abundance of cooperatively acting hydrogen bonds that can readily break and reform.[36–38] In this context, PVA, which has pendant hydroxyl groups capable of both hydrogen-bond-accepting and -donating, can serve as a link between adjacent DWNT bundles by forming hydrogen bonds with the carboxylic acids and esters present in the polymer coating of the DWNT bundles.

As shown in our previous work,[31] spinning a ribbon of DWNT bundles produces a sequence of buckles that transform the ribbon into a filamentary yarn, with the buckles acting as filaments. By twisting the CNT ribbons into yarns, the edges of the CNT ribbon are overlaid on each other, preventing a premature failure of the DWNT network at the edges.[43] During the spinning process, an axial force develops in the yarn, which, due to the twisted morphology of the yarn, generates significant lateral contraction. This, together with the lower mobility of the adsorbed PVA macromolecules (relative to DMSO molecules) and good interactions between PVA and the inherent polymer coating, squeezes the excess DMSO solvent out of the twisted structure. The spinning also compacts the DWNT bundle network, increasing the density by about 50 times, from approximately 0.03 to 1.5 g/cm^3. After fabrication, residual solvent was removed by heating the yarns at 150 °C for 12 h under vacuum.

Yarn Morphology. As described previously,[31] the surface morphology of a yarn synthesized from the MER

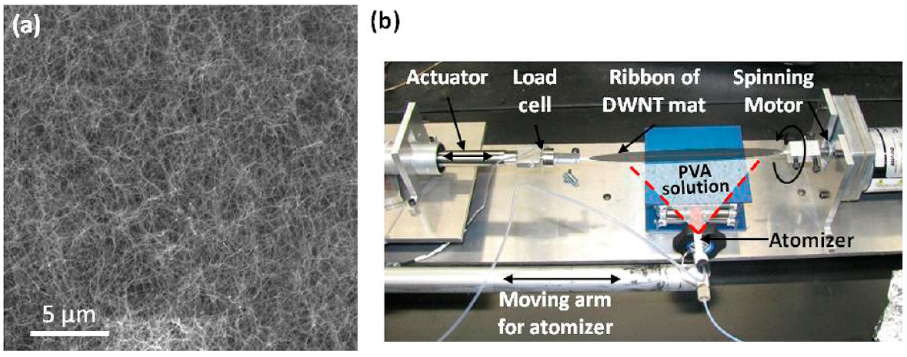

Figure 3. (a) Porous mat of DWNT bundles. (b) Custom-made spinning system for fabrication of the DWNT−PVA composite yarns presented in this study. A ribbon of the DWNT mat is clamped between the load cell (attached to a linear actuator) and spinning motor, and subsequently spun by the spinning motor and axially stretched by the actuator. Simultaneously to being twisted and stretched, the yarn is sprayed with the PVA solution from the atomizer, which moves along the full length of the yarn.

DWNT mats resembles that of a macroscopic yarn fabricated by twisting a series of filaments together. However, the filament-like structure of the yarn corresponds to buckled sections of the original mat, deformed as a result of the compressive stresses caused by the twisting moment during spinning. This twisted filament-like structure enhances the ductility and energy to failure of the yarns, without sacrificing strength,[31] by spreading inelastic deformation over the entire yarn length.

The as-produced DWNT mat is over 98% porous (Figure 3a), as estimated based on the ratio of the volume density of the mats, ρ_{mat}, to the volume density of the DWNTs in a hexagonally close-packed structure, ρ_{CNT} = 1.575 g/cm^3, (Porosity = 1 − ρ_{mat}/ρ_{CNT}).[31] Spinning the mat into DWNT−PVA yarn results in a substantial increase in density (fracture surfaces are shown in Figure 4).

In addition to the surface morphology and yarn porosity, insight into the yarn organization and interactions between the PVA matrix and DWNT phase is obtained by examining the fractured surfaces of yarns of varying PVA content (Figure 4). The yarns without any PVA exhibit a macroscopically semibrittle failure, in that the folded mat breaks along a single plane perpendicular to the loading axis, and all adjacent folds of the mat appear to have broken simultaneously. Bundles of DWNTs that have pulled out from the surrounding mat are visible throughout the fractured surface. In addition, the fracture surface reveals porosity in the yarn as the adjacent wrinkles of the mat are not in contact with each other; thus, little to no direct load transfer could occur between adjacent layers of the twisted mat. The fracture surface of a 9 wt % PVA yarn shows a macroscopic mixed-mode failure, with a more macroscopic shear failure. In particular, it is noted that there appears to have been a cooperative deformation between neighboring mat surfaces, where adjacent mat surfaces may have failed at different times, as the load was transferred from one layer of mat to an adjacent layer leading up to final yarn failure. Thus, filling in the voids with the added PVA appears to provide a pathway for load transfer between adjacent folds of the twisted mat within the yarn. In the yarn with 31 wt % PVA, a macroscopic shear failure is observed, as the fracture surface is inclined approximately 45° from the yarn tensile axis. More notably, examination of the three fracture surfaces in Figure 4 reveals a decreasing porosity in the yarn with added PVA, as the PVA has filled the gaps between the layers. We note that at high PVA contents, PVA chains can form agglomerations that are not readily distinguishable using scanning electron microscopy (SEM). Such agglomerates could adversely affect the mechanical behavior of these high-PVA-content yarns by providing weak localized regions in the yarn where fracture initiation may occur.

Mechanical Properties. Mechanical properties were measured through quasi-static tensile tests performed on 16 mm gauge length yarns (see Materials and Methods section). The stress in each yarn was calculated by dividing the measured force by the load-bearing cross-sectional area of the yarn, which includes the areas of the CNTs, PVA, and inherent polymer coating, as described in the Materials and Methods section.

It should be emphasized that, due to a lack of standardized techniques for measuring mechanical properties of CNT-based yarns, it is difficult to directly compare measurements reported in the literature, which vary greatly depending on gauge lengths, strain rates, and cross-sectional area definitions. Among these variables, the most important discrepancy is in the determination of the yarn cross-sectional area. As pointed out by Windle and co-workers,[44] the often-employed technique for calculating the mechanical properties of CNT-based yarns from diameter measurement in the SEM does not provide good accuracy, partly due to significant porosity within the yarns. Therefore, the properties are often reported by

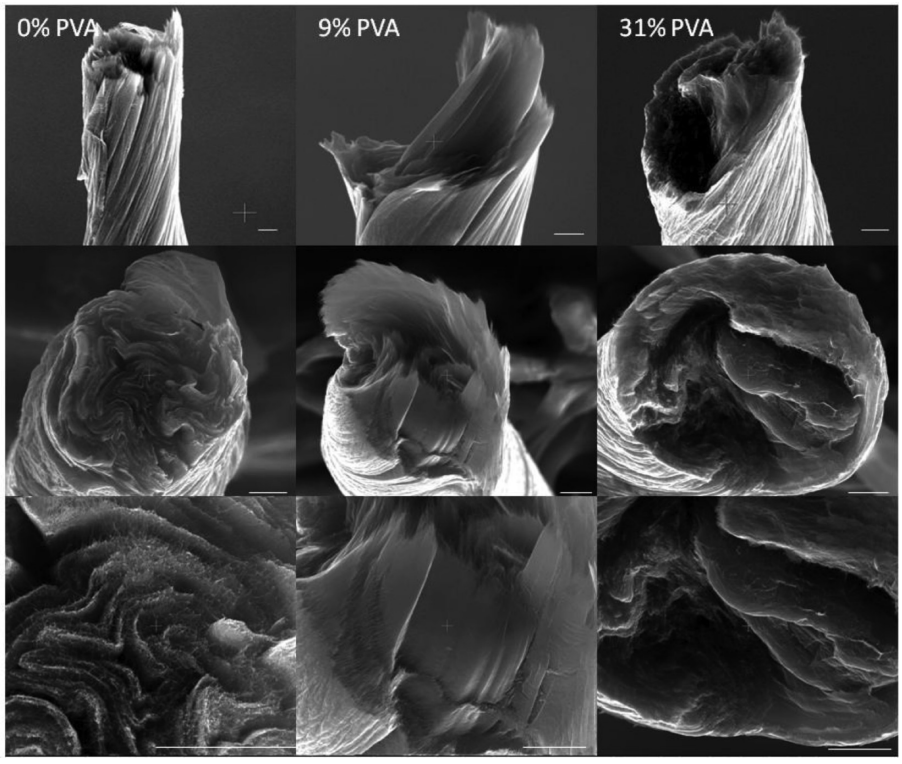

Figure 4. SEM images of fracture surfaces for DWNT–PVA composite yarns containing 0, 9, and 31 wt % PVA. All scale bars 10 μm.

measuring the yarn linear density, and dividing by an assumed volumetric density to obtain the area.[44,45] In particular, a density of 2.0–2.25 g/cm^3, which is in the range of typical carbon fibers and graphite, is often assumed.[46–51] In this work, we use a density of 1.575 g/cm^3, which corresponds to hexagonally close-packed DWNTs in a bundle[31] and is more relevant to the MER DWNTs. To emphasize the importance of using an accurate density value, if one assumes a density of 2.25 g/cm^3, the calculated stress would be 40% higher than the value obtained using a density of 1.575 g/cm^3. In addition, we calculate the cross-sectional area for each yarn individually, incorporating the cross sectional area of the CNTs, the PVA, and the inherent polymer coating, (see Materials and Methods section) so as to be rigorous in quantifying the mechanical properties of individual yarns.

Representative stress–strain curves for yarns without any polymer, and with 9 wt % PVA are shown in Figure 5. For each yarn, the modulus is calculated as the initial slope of the stress–strain curve, and the energy to failure is calculated as the area under the force-strain curve divided by the linear density. The stress is calculated as the engineering stress, or maximum force divided by initial effective cross-sectional area. The global strain to failure in these yarns is approximately 15–20%. Comparisons of these three properties as a function of PVA content in the yarns (Figure 6) show parabolic dependences of stiffness, or modulus, and energy to failure on the PVA content. In particular,

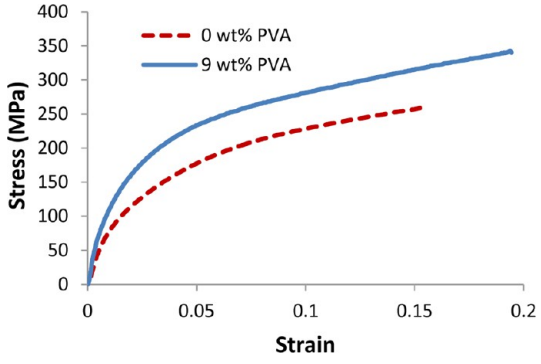

Figure 5. Representative stress–strain curves for DWNT–PVA composite yarns with 0 and 9 wt % PVA.

these plots show that all three measured mechanical property values increase with PVA content up to ~12 wt % PVA, with the average specific modulus increasing by 59%, the average energy to failure increasing by 49%, and the average specific strength increasing by ~33%. Addition of PVA beyond that point leads to a decrease in stiffness and energy to failure, and no change in strength, suggesting a possible optimal PVA content, or hydrogen bond density (see Molecular Dynamics Simulations section), which provides a network through which the shear interactions between adjacent bundles are increased at both small deformations, resulting in increasing stiffness, and large deformation, resulting in an increase of energy to failure. Interestingly, all of the yarns produced with ~30 wt % PVA failed during fabrication, before reaching the

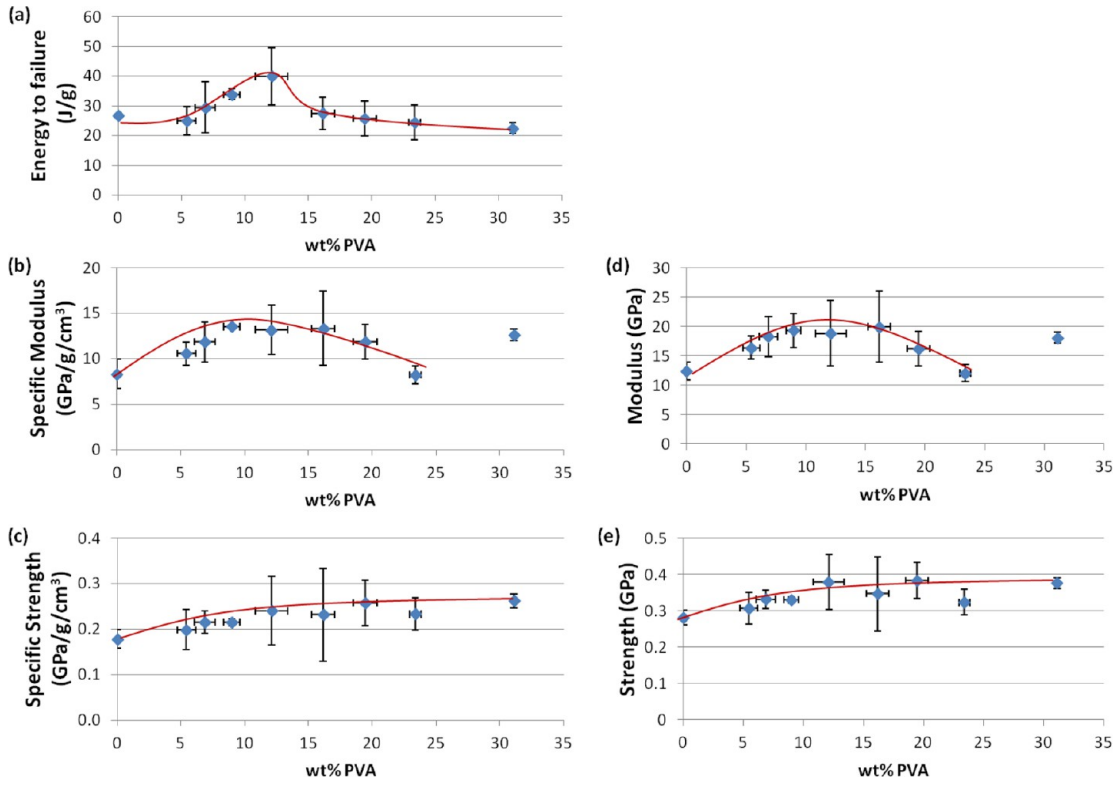

Figure 6. Mechanical properties of CNT composite yarns as a function of PVA: (a) energy to failure, (b) specific elastic modulus, (c) specific ultimate strength, (d) absolute modulus, and (e) absolute strength. Each data point represents an average for at least 3 tests, with the vertical error bars indicating the standard deviation of the mechanical property, and the horizontal error bars indicating the standard deviation of the PVA content for the associated tests. The red curves are guides for the eye.

standard number of turns per yarn. This is likely due to PVA agglomerates forming in the yarns during fabrication with high concentration PVA solutions. These agglomerations may serve as weak points in the yarn, leading to premature failure during twisting and stretching of the yarn. Therefore, while we report the measurements for these yarns for completeness, we suspect that their properties may not represent those of a yarn with uniform diameter and PVA content along its full length.

Figure 6 presents the average values measured in this study. For comparative purposes, the highest properties measured were: a strength of 0.54 GPa and an energy to failure of 70.4 J/g in a yarn containing 13 wt % PVA, and a modulus of 30.6 GPa in a yarn containing 12 wt % PVA. These properties are calculated with respect to the yarn cross-sectional area containing the CNTs, PVA, and polymer coating. When only the area of the CNTs, which are responsible for carrying the vast majority of the load, is used, these properties translate to a strength of 0.77 GPa, an energy to failure of 100.7 J/g, and a modulus of 42.8 GPa. This second calculation is performed solely to determine the effectiveness of the PVA in increasing the load transfer between CNTs. In particular, it should be noted that PVA films themselves have strength values between ~27 and 81 MPa, and Young's Modulus values of ~1.8–1.9 GPa;[52,53] thus, the PVA is an inherently weak component compared to the CNTs. Table 1 reports all of the average mechanical properties for the yarns in tension, with respect to both of the above-referenced cross-sectional areas, as well as well as the maximum measured values.

While the focus of this work is to investigate the effect of increasing PVA, and therefore increasing hydrogen-bond density, on the mechanical properties of DWNT–PVA yarns, we note that the values obtained in this study are in line with those reported in the literature. We also note that the load-bearing area calculations used in the below cited literature vary from entire cross-sectional area to CNT-only area, thus direct comparison between all values cannot be made. However, these values are provided as examples of reported mechanical property measurements in various fiber and CNT-based systems. The toughness values measured in this study are comparable to or higher than the toughness of heat treated Nylon fibers (1–7 J),[54] many high-toughness CNT based yarns (30–100 J/g),[31] Kevlar (30 J/g),[55] and graphite fibers (12 J/g).[56] In addition, the strength of DWNT–PVA yarns (specific strength of 0.2–0.3 GPa/g/cm^3 equivalent to 0.3–0.4 GPa) is significantly higher than that exhibited by CNT-reinforced polymer composites that contain *randomly oriented* CNTs, even at relatively high CNT concentrations. Examples of these systems are: single wall nanotubes (SWNT)–PVA composites

TABLE 1. Measured Mechanical Properties as a Function of PVA Content, Where *Engineering Values* Correspond to Those Calculated Using the Full Cross-Sectional Area of the CNTs, Polymeric Coating, and PVA, and *True Values* Correspond to Those Calculated Using the Cross-Sectional Area of the CNTs Only

	engineering values (area of CNT, polymer coating, PVA)			true values (area of CNT only)		
PVA content (wt%)	energy to failure (J/g)	modulus (GPa)	strength (GPa)	energy to failure (J/g)	modulus (GPa)	strength (GPa)
0	26.8 ± 0.9	12.4 ± 1.5	0.28 ± 0.02	31.6 ± 5.7	16.8 ± 4.4	0.34 ± 0.05
5.4 ± 0.7	25.0 ± 4.8	16.4 ± 2.0	0.31 ± 0.04	34.6 ± 9.0	20.8 ± 3.2	0.39 ± 0.06
6.9 ± 0.8	29.4 ± 8.6	18.3 ± 3.4	0.33 ± 0.02	30.4 ± 1.1	21.9 ± 5.1	0.43 ± 0.06
9.0 ± 0.6	33.8 ± 1.8	19.4 ± 2.9	0.33 ± 0.01	43.3 ± 6.0	26.1 ± 3.2	0.44 ± 0.02
12.1 ± 1.3	40.0 ± 9.7	18.8 ± 5.6	0.38 ± 0.08	54.0 ± 17.6	25.5 ± 6.1	0.57 ± 0.12
16.2 ± 0.9	27.5 ± 5.4	20.0 ± 6.1	0.35 ± 0.10	40.8 ± 8.4	29.9 ± 9.5	0.52 ± 0.16
19.5 ± 0.9	25.7 ± 5.9	16.2 ± 2.9	0.38 ± 0.05	40.3 ± 9.2	26.6 ± 3.6	0.60 ± 0.08
23.4 ± 0.5	24.4 ± 5.9	12.1 ± 1.5	0.32 ± 0.04	40.6 ± 9.6	20.1 ± 2.4	0.57 ± 0.08
31.1	22.4 ± 1.9	18.1 ± 0.9	0.38 ± 0.02	42. ± 3.6	34.3 ± 1.7	0.71 ± 0.03
Maximum values	70.4	30.6	0.54	100.7	42.8	0.77

fabricated by soaking buckypaper of SWNTs in PVA solution resulting in a strength of 57 MPa for ~25–30 wt % of polymer content,[6] SWNT-PVA composites fabricated by dispersing CNTs in PVA solution providing strength in the range of 83–150 MPa for up to 5 wt % of CNTs,[16] MWNT-polymer composites fabricated by shear mixing resulting in strength of ~40 MPa for up to 25 wt % of MWNTs,[57] and MWNT-polymer composites fabricated using a layer-by-layer (LBL) assembly technique resulting in strengths of 150 ± 35 MPa, for up to 50 wt % of CNTs in the composite.[58,59] We note that while CNT-based nanocomposites with higher strengths have also been reported,[8,15,42,45] albeit with reduced strain-to- failure, the CNTs in these studies were partially or fully aligned with the loading direction, pointing to the importance of filler alignment on load transfer in nanocomposites. As such, it is worth emphasizing here that our DWNT–PVA yarns are mostly composed of randomly oriented CNTs, primarily due to the difficulties associated in aligning CNTs inside the CVD reactor, and subsequently during spinning of yarns from the CNTs due to entanglements developed between CNTs inside the reactor.

As pointed out by Koziol *et al.*,[60] the mechanical properties of CNT-based yarns have significant statistical variation due to the randomized presence of weak points along the testing gauge length, attributable to imperfections introduced during manufacturing. In our study, the variations may be attributed to several factors, including: (i) slight variations in mat areal density prior to twisting the cut ribbon into a yarn, (ii) slight variations in the ribbon width along the length that result in diameter variations in the fabricated yarn, and (iii) localized PVA agglomerations introduced during the polymer infiltration. The lower stiffness and energy to failure of the PVA–CNT yarns at higher concentrations of PVA may be explained in part by the formation of PVA-only domains in the composite yarns. These domains of weaker material may serve as defects at which failure can initiate, decreasing the energy to failure of the yarns.

The enhanced mechanical properties of our DWNT–PVA yarns can be attributed to an excellent network of hydrogen bonds between the PVA matrix and the inherent polymer coating on the DWNTs. Infiltration of the DWNT yarns with PVA provides an avenue for interaction between the coated DWNTs: the PVA chains interact with the inherent polymer coating on the DWNT bundles through hydrogen bonds, and may unfold and stretch with macroscopic large deformation of the yarn. These hydrogen bonds can be broken and reformed easily in response to large mechanical deformation, providing structural integrity to the yarn over large deformations and thus enhanced toughness, or energy to failure, compared to yarns without PVA. This load-transfer mechanism is similar to those that exist in natural materials such as spider silk and collagen, whose high toughness and strength come from a synergistic interplay between both stiff and compliant building blocks.[36,38]

Molecular Dynamics Simulations. To uncover the deformation mechanisms present at the nanoscale, we performed molecular dynamics (MD) simulations of shearing adjacent CNTs to calculate the interface stiffness as a function of added PVA. Our system consists of two CNTs, each with an outer diameter of 1 nm and a length of 4 nm. Molecules of the inherent polymer coating are covalently attached to the tube walls and are represented by 4-mer poly(methyl methacrylate) (PMMA) chains[61] with 50% hydrolyzed ester groups to introduce hydrogen bond donors and acceptors. As shown in Figure 7, the bottom CNT is fixed in space, and a spring, with stiffness k_{SMD}, is attached to one end of the top CNT, and pulled at a velocity v, thus shearing the interface between the CNTs.

To study the effect of PVA content on interface stiffness, the following PVA contents are introduced: 0, 5, 10, 20, 40, and 60 wt % (Figure 7). In the cases of 5, 10,

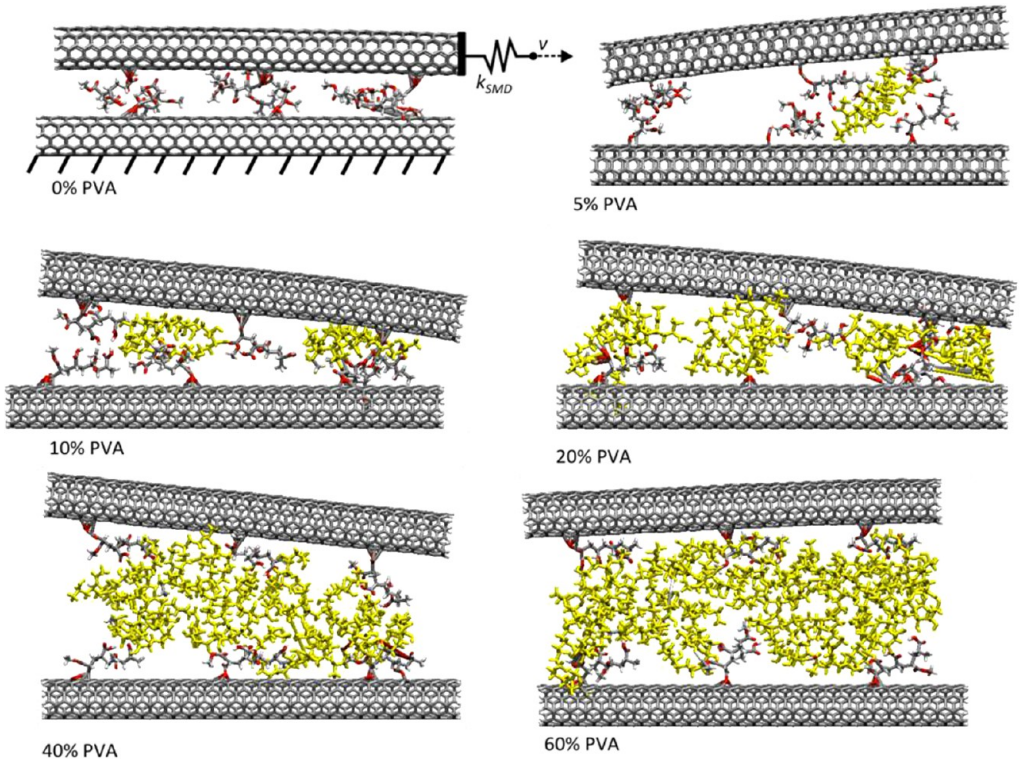

Figure 7. Snapshots of equilibrated systems used in MD simulations showing carbon nanotubes with inherent polymer coating and varying PVA (yellow) content from 0 to 60 wt %. The bottom CNT is fixed and top CNT is pulled to perform a shear test.

and 20 wt % PVA, a monolayer of PVA is formed between the CNTs, whereas for 40 and 60 wt % PVA, a finite thickness of PVA results between the CNTs. Note that these weight percentages do not map directly to the weight percentages of PVA measured in the experiments where the PVA is assumed to coat bundles of CNTs as the PVA is assumed in the MD simulations to only be present between single CNTs (see Materials and Methods section and Table 2). All systems are equilibrated at 300 K using an *NVT* (constant number of particles, volume, and temperature) ensemble, during which the bottom CNT is fixed, and the top CNT is confined to remain in the plane. During the shearing simulations, the force *versus* displacement behavior is recorded (Figure 8a), and the stiffness is calculated as the slope of the recorded curve over the first 10 Å of displacement.

Our simulations reveal that the introduced PVA interacts strongly with the polymeric coatings on the CNTs, and serves to link the adjacent CNTs. A comparison between the interface stiffness measured in simulations and the yarn modulus measured in experiments, based on similar thickness of PVA between tubes or bundles, is given in Figure 8c. In addition, the number of *productive* hydrogen bonds, defined as the number of hydrogen bonds between the inherent functionalization and the PVA only, is calculated at the start of each simulation, and increases with increasing PVA content (Figure 8d). As the PVA content is increased such that the PVA thickness exceeds a monolayer between the CNTs, the stiffness decreases.

TABLE 2. Approximate Correlation between MD System Weight Percentage of PVA and Experimental Weight Percentage of PVA

MD system wt % PVA	experimental wt % PVA
0	0
5	3
10	5
20	11
30	18
40	25
60	43

We note that the hydrogen bond strength between the PVA molecules is equivalent to that between the PVA molecules and the inherent polymer coating molecules (5 kcal/mol),[62] but the number of hydrogen bonds present in the systems increases with added PVA (Figure 8d), resulting in disparate deformation mechanisms for small and large amounts of PVA. When small amounts of PVA are present (*e.g.*, 10 wt % or less), there are only a few hydrogen bonds between the PVA molecules themselves, and the PVA forms a monolayer. However, as the PVA content increases to a substantial amount (*e.g.*, ~60 wt %), there are numerous hydrogen bonds between the PVA molecules themselves (Figure 8d), as the PVA forms a finite thickness layer between the CNTs. For the case of 10 wt % PVA, during

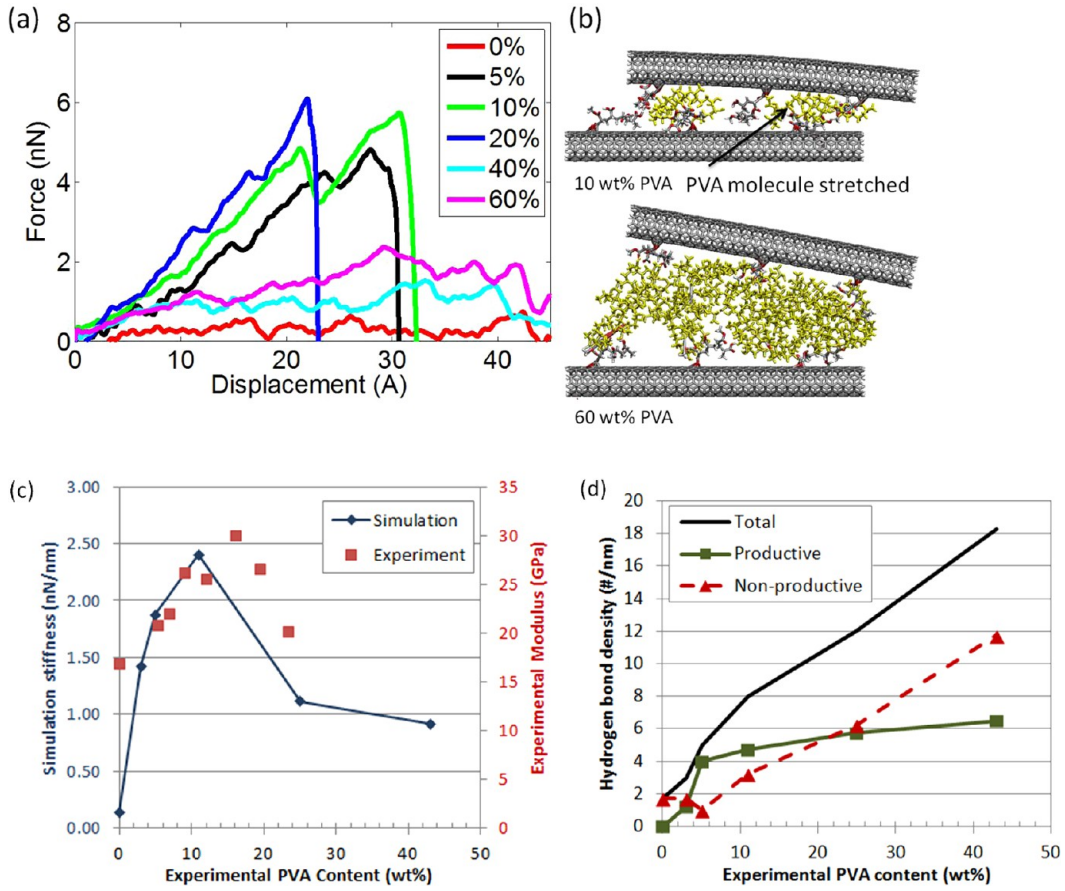

Figure 8. (a) Force displacements relations for different PVA content. The interfacial stiffness for each system is calculated as the slope of the force-displacement curve over the first 10 Å of displacement. (b) Snapshots of MD simulations for 10 wt % PVA (top) and 60 wt % PVA (bottom) at an applied shear displacement of 9 Å. In the case of 10 wt % PVA, the PVA molecules stretch, while in the case of 60 wt %, the higher compliance of the interface allows for deformation without stretching of individual PVA molecules. (c) Stiffness calculated through MD simulations as a function of PVA content compared with modulus measured experimentally. The stiffness increases as the PVA content increases and then drops as observed in experiments. (d) The total hydrogen bond density compared with the productive and nonproductive hydrogen bond densities calculated through MD simulations. Note that the drop in stiffness *versus* PVA content found through MD simulations corresponds to the PVA content at which nonproductive hydrogen bonds exceed productive hydrogen bonds.

the initial applied displacement of the top CNT, the deformation is accommodated by the stretching of the small number of interior PVA molecules, leading to the uncoiling and stretching of the PVA monolayer (Figure 8b). Conversely, for the case of 60 wt % PVA, it is observed that with applied displacement of the top CNT, the hydrogen bonds between the PVA molecules themselves break and reform (Figure 9), precluding stretching of the individual PVA molecules. Thus, the applied deformation is accommodated through shear deformation of the thicker and more compliant polymer interface rather than uncoiling of individual PVA molecules.

Through the MD simulations, we also compute the total number of hydrogen bonds for the cases of 10 and 60 wt % PVA as a function of applied shear displacement of the top CNT. As shown in Figure 9, the number of hydrogen bonds in each of these systems is not constant, but rather it fluctuates with applied deformation. This indicates that in this

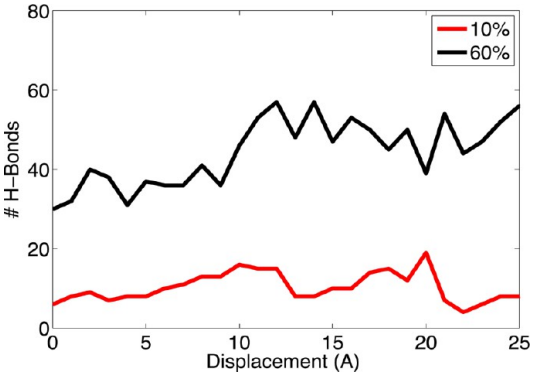

Figure 9. Number of hydrogen bonds *versus* shear displacement applied to top CNT in MD simulations for the cases of 10 and 60 wt % PVA. The evolution of hydrogen bonds *versus* displacement indicates that hydrogen bonds do break and reform with deformation in the PVA-CNT-inherent coating system.

CNT-PVA-inherent polymer coating system, hydrogen bonds do break and reform to accommodate the

applied deformation. In addition, it is noted that over the first 10 Å of applied displacement, where the interfacial stiffness is calculated, more hydrogen bonds break and reform in the case of 60 wt % PVA as compared to 10 wt % PVA. This demonstrates that for the cases of large amounts of PVA, the hydrogen bonds within the PVA system itself break and reform to accommodate the applied deformation, resulting in increased interfacial compliance.

Figure 8d is used to determine if the optimization in interfacial stiffness observed in MD simulations can be explained by an optimal hydrogen bond density. The productive hydrogen bond density increases sharply with the addition of up to 10 wt % PVA in the simulations (~5 wt % experimental PVA content). Addition of PVA beyond this provides small increases in productive hydrogen bond density, and much higher increments in added nonproductive hydrogen bond density. Thus, the transition from increasing interface stiffness to decreasing interface stiffness as a function of PVA content in the MD simulations corresponds to the point at which the nonproductive hydrogen bonds exceed the productive hydrogen bonds.

The MD simulations show that a small amount of PVA is effective in linking the adjacent tubes through hydrogen bonds with the inherent polymer coating on the surface of the tubes, thus providing rigidity to the tube–tube interface. The more gradual addition of productive hydrogen bonds, or the dominance of nonproductive hydrogen bonds, corresponds to the decreasing interfacial stiffness. Thus, once an optimal PVA content, or hydrogen bond density, has been exceeded, the PVA forms noncooperative bonds with neighboring PVA molecules, making the interface more compliant, thus decreasing the stiffness of the interface.

CONCLUSIONS

In this study, we have demonstrated an approach by which lessons from nature can be incorporated into the design of polymer–DWNT nanocomposite yarns. Importantly, we showed that the inherent polymer coating present on the surface of CVD-synthesized DWNT bundles can be exploited in the development of polymer–DWNT yarns with better mechanical properties than yarns that are made from DWNTs alone. As the polymer coating on the DWNT bundles contains both hydrogen-bond donor and acceptor groups, nature's design strategy, in which stiff components can be linked together through a network of weak hydrogen bonds that can break and reform with deformation, can be implemented with the addition of a small amount of flexible polymer. The introduction of PVA, which mediates a dense network of hydrogen bonds between the CNT bundles, affords high stiffness, strength, and energy to failure to macroscopic DWNT-based yarns. These hydrogen bonds work cooperatively to transfer loads, break and reform with deformation, thus providing a mechanism for increased energy to failure.

The systematic study that we present herein serves to elucidate the effect of increasing hydrogen bond density on the macroscopic mechanical properties. The experimental results point to parabolic relationships between the PVA content in the yarn and both the energy to failure and stiffness, which we confirmed with molecular dynamics simulations. These results clearly point out an optimal PVA content, where the PVA chains provide a sufficient number of hydrogen bonds to directly link, and successfully transfer the load between, adjacent DWNT bundles. Addition of PVA beyond this optimal content results in PVA–PVA regions that serve as weak points in the yarn, where hydrogen bonding occurs only between PVA molecules and does not strengthen the interactions between adjacent DWNT bundles.

Lastly, we have demonstrated a comprehensive synthetic-measurement-modeling strategy for achieving improved macroscopic mechanical properties of DWNT–PVA nanocomposite yarns as a function of the chemistry between functionalized CNTs and an interacting polymer matrix. While the yarns fabricated here are composed of mostly randomly oriented CNTs, the insight gained from the multidisciplinary approach presented here can be used to develop higher-performance yarns when utilized with optimal fabrication techniques that produce yarns with highly aligned CNTs.

MATERIALS AND METHODS

Materials. DWNT mats were produced at the Materials and Electrochemical Research (MER) Corporation (Tucson, AZ). Polyvinyl alcohol (PVA, 30 000–70 000 MW, 87–90% hydrolyzed) and dimethyl sulfoxide (DMSO, 99%) were obtained from Sigma-Aldrich (Milwaukee, WI).

Characterization. ^{1}H and ^{13}C NMR spectra were collected on an AVANCE III 500 MHz NMR system located in the Integrated Molecular Structure Education and Research Center (IMSERC) at Northwestern University. TGA was performed in the Polymer Characterization Laboratory at NU using a Mettler-Toledo TGA/SDTA851 instrument with samples heated from 50 to 800 °C in a N_2 and air atmosphere with a scanning rate of 10 °C/min.

Fabrication of CNT Based Yarns. As-produced DWNT mats are highly porous with a density of ~0.04 g cm^{-3}. To increase the density of the mat and to develop the efficient load transfer between DWNT bundles, the mats were spun into yarns. A spinning system was developed to fabricate DWNT–PVA composite yarns. The system is composed of four main components (Figure 3b): actuator, spinning motor, load cell, and atomizer. These components respectively stretch the CNT yarn, twist it, measure the axial load, and spray polymer solutions on the sample during spinning.

The CVD grown mats of DWNT bundles were cut into 1/4 in.-wide ribbons. One end of the ribbon was attached to the spinning motor, and the other end was gripped to the load cell connected to the linear actuator. The actuator provides tensile stretching of the ribbon at a rate of 20 μm s^{-1}, while the ribbon is simultaneously spun by the spinning motor for a final number of turns of 3 turns/mm of ribbon length. The load cell monitors the forces generated. By measuring and limiting the force in the CNT ribbon during spinning, premature failure of the ribbon due to excessive spinning/stretching is prevented. During spinning, a solution of PVA in DMSO is sprayed onto the yarn using an atomizer. The PVA content was controlled by varying the PVA solution concentration from 0.01 to 5.0 wt %.

The process of twisting DWNT ribbons into yarns induces compressive stresses in the plane of the mat, causing the mat to buckle. Initially, the twisting of the yarn is not uniform along the length of the ribbon due to varying torsional stiffness along the ribbon, which could be a result of local variations of the mat porosity in different locations. However, upon further twisting, the portions of the ribbon with higher twist gain torsional rigidity, allowing for the applied twist to be transferred to other portions of the yarn, thus yielding yarns with relatively uniform cross sections and twists.

The yarns are then heated in a vacuum oven at 150 °C overnight, followed by storage in a humidity controlled (20%) vacuum chamber overnight. This treatment is to ensure all of the solvent is removed from the yarns before mechanical tests. In addition, the humidity during the tests is controlled to remain at ~20% to remove any effect of moisture on the yarn properties. This is critical in improving the fidelity of the experiments, as water contents in air may alter the hydrogen bond formation.

Analysis of Inherent Polymer Coating *via* Extraction. A segment of DWNT mat (~3 cm long, and 1/4 in. wide) containing CNT bundles and the inherent polymer coating was placed in a 12 mL PTFE-capped glass vial in methyl ethyl ketone (5 mL) and sonicated in a bath sonicator (Fisher Scientific FS60, 150 W) for 2 h to remove the polymer sizing. This process disintegrates the yarn into smaller masses of CNT bundles, which become suspended in the solvent and can be separated from the solution by passage through a 0.22 μm syringe filter. The collected solution was evaporated by rotary evaporation to yield a white film of polymer coating that can be readily dissolved in deuterated acetone for NMR analysis.

Analysis of PVA Content in Yarns. Each manufactured yarn, approximately 3 in. in length, was cut into three pieces so that three mechanical tests could be performed from each of the fabricated yarns. After each mechanical test was complete, the two fractured segments from a single specimen were evaluated for PVA content. First, the linear mass density (mass/length) of the two fractured segments was calculated, using a Mettler-Toledo microscale with an accuracy of 0.2 μg to weigh each segment. The uniformity of the linear density along the length of the yarn was checked by comparing the measured linear densities for the fractured segments. Samples with uniform linear density (±10%) were evaluated for PVA content. For this purpose, the two fractured DWNT/PVA yarn segments were pyrolyzed at 800 °C (ramp rate 10 °C/min to 800 °C) under the flow of ultrahigh pure argon gas in a high temperature vacuum tube furnace (GSL 1100) purchased from MTI Corporation (Richmond, CA). The tube furnace was purged with Ar for 2 h prior to pyrolysis. The oxygen content during the pyrolysis was monitored by an oxygen analyzer (W3000) also purchased from MTI Corporation, attached to the tube furnace. The PVA concentration (wt %) was calculated from the difference of the masses before and after pyrolysis, taking into account the fact that the inherent polymeric coating is also burned off during pyrolysis.

Mechanical Testing. The mechanical properties of the DWNT–PVA composite yarns were measured using a microtensile testing frame (Fullam 2000 lb testing frame) equipped with a 2.5 N load cell with 2 mN resolution (Honeywell model 31) and a linear variable differential transformer (LVDT) with a displacement resolution of 1 μm (Allison model HS50). The yarns were fixed to end tabs using an epoxy glue, and the end tabs were gripped for mechanical testing.

Each yarn sample had a gauge length of approximately 16 mm, and was loaded in tension at a rate of 0.2 mm/min, providing a quasi-static strain rate on the order of 2×10^{-4} s^{-1}. The average yarn engineering tensile strain was calculated as the crosshead displacement divided by the yarn gauge length, with a strain resolution of ~0.01%.

Loading Area Calculation of CNT Based Yarns. The loading area of the yarns is calculated to account for the cross-sectional area of the CNTs, the inherent polymeric coating, and the PVA, which are the components in the yarn that carry the load. We note that there is not a standard for defining the cross-sectional area in CNT-based yarns, and therefore, it is difficult to directly compare strength, stiffness, and energy to failure measurements between reports in the literature.[63]

As mentioned in the previous section, we measure the PVA content for each yarn. From the TGA of the mats (see Figure S1 in Supporting Information) and SEM, it is determined that the mats used in this study were composed of 12 wt % polymeric coating, 22 wt % Fe, 6 wt % nontube (amorphous and graphitic) carbon, and 60 wt % DWNT, from which we calculate the linear densities of each component in each yarn segment. We assume that the catalyst particles do not participate in carrying the load,[31,64] and thus exclude them from the calculation of load-bearing cross-sectional area. Therefore, the loading area is calculated as:

$$A_{\text{effective}} = \frac{\lambda_{\text{CNT}}}{\rho_{\text{CNT}}} + \frac{\lambda_{\text{Coating}}}{\rho_{\text{Coating}}} + \frac{\lambda_{\text{PVA}}}{\rho_{\text{PVA}}} \quad (1)$$

where we assume ρ_{CNT} = 1.575 g·cm^{-3}, corresponding to hexagonally close packed DWNT,[31] and ρ_{PVA} = 1.2 g·cm^{-3}. The density of the intrinsic polymer coating is assumed to be the same as the CNTs, as it is conformal to the surface of the CNT bundles, $\rho_{\text{Coating}} = \rho_{\text{CNT}} = 1.575$ g·cm^{-3}. The terms λ_{CNT}, λ_{Coating}, and λ_{PVA} are the calculated linear densities of the CNTs, coating, and PVA in the yarns.

As noted previously, a more relevant comparison between studies introducing some weak polymer into the stiff CNTs is to use the cross-sectional area of the CNTs only. This affords a more accurate description of how effectively the CNTs are involved in the load transfer, by providing a way to determine if adding a particular polymer successfully engages more of the outstandingly high mechanical performance of individual CNTs, while also excluding uncertainties related to the amount and properties of other DWNT–PVA components, in particular occurring with the mixed-matrix composites, like in the present case of combining the intrinsic polymer coating matrix with the external PVA matrix . Therefore, the mechanical property values we report considering the area of the CNTs only by utilizing the following equation:

$$A_{\text{CNT}} = \frac{\lambda_{\text{CNT}}}{\rho_{\text{CNT}}} \quad (2)$$

Calculation of PVA Thickness in Experiments and MD Simulations. Because of computational limitations, a full atomistic simulation corresponding to two adjacent bundles of DWNTs, measuring >20 nm in diameter, cannot be carried out. Therefore, in order to relate the experimental results to the computational simulation, we estimate the relevant PVA thickness in the experiments that would need to be simulated for comparison between experiment and simulation.

Assuming that in the experiments the PVA uniformly coats the bundles, the thickness of PVA, $t_{\text{PVA,experiment}}$, can be approximated as:

$$t_{\text{PVA,experiment}} \approx \frac{m_{\text{PVA}}}{l \rho_{\text{PVA}} \pi D_{\text{bundle}}} \quad (3)$$

where D_{bundle} is the diameter of the bundle, which can range from ~10 to 30 nm, m_{PVA} is the mass of the PVA, and l is the length of the tube that the PVA is coating.

In the simulations, the PVA is located in a region between the tubes approximately w = 1 nm wide (corresponding to the

width of the CNT) and l = 4 nm long (length of the CNT in the model); thus, the thickness is approximated as

$$t_{PVA,MD} \approx \frac{m_{PVA}}{\rho_{PVA} \cdot l \cdot w} \quad (4)$$

Equating the thickness between tubes given by eqs 3 and 4 provides the relationship between the experimental PVA weight percentages and those in the MD simulation system given in Table 2.

MD Simulations. A series of full atomistic simulations of the mechanical test was implemented *via* classical molecular dynamics (MD). The MD simulations were performed using the massively parallelized modeling code LAMMPS,[65] capable of running in parallel on large computing clusters. We use the ReaxFF force field to describe the chemical and mechanical behavior of hydrocarbons, carbon nanotubes and other carbon structures to near quantum mechanical accuracy.[62] Shearing of the CNTs interface was performed using Steered Molecular Dynamics (SMD). The top CNT is loaded by a virtual spring with a deformation rate given by a dummy atom velocity corresponding to a loading rate of 150 pN/ps. The loading rate of 150 pN/ps was chosen for all shearing simulations after a parametric study and to optimize computational efficiency without sacrificing data fidelity.

Conflict of Interest: The authors declare no competing financial interest.

Supporting Information Available: TGA of the DWNT mats. This material is available free of charge *via* the Internet at http://pubs.acs.org.

Acknowledgment. This research was funded by the ARO-MURI program (Award No. W991NF-09-1-0541). H.D.E. gratefully acknowledges support from ONR through Award No. N00014-08-1-0108. S.B.N. acknowledges the support from the NSF (Award No. DMR-0520513 through the Materials Research Science and Engineering Center at Northwestern University).

REFERENCES AND NOTES

1. Yu, M. F.; Files, B.; Arepalli, S.; Ruoff, R. Tensile Loading of Ropes of Single Wall Carbon Nanotubes and Their Mechanical Properties. *Phys. Rev. Lett.* **2000**, *84*, 5552–5555.
2. Peng, B.; Locascio, M.; Zapol, P.; Li, S.; Mielke, S. L.; Schatz, G. C.; Espinosa, H. D. Measurements of Near-Ultimate Strength for Multiwalled Carbon Nanotubes and Irradiation-Induced Crosslinking Improvements. *Nat. Nanotechnol.* **2008**, *3*, 626–631.
3. Lima, A. M. F.; Musumeci, A. W.; Liu, H. W.; Waclawik, E. R.; Silva, G. G. Purity Evaluation and Influence of Carbon Nanotube on Carbon Nanotube/Graphite Thermal Stability. *J. Therm. Anal. Calorim.* **2009**, *97*, 257–263.
4. Pang, L. S. K.; Saxby, J. D.; Chatfield, S. P. Thermogravimetric Analysis of Carbon Nanotubes and Nanoparticles. *J. Phys. Chem.* **1993**, *97*, 6941–6942.
5. Pop, E.; Mann, D. A.; Goodson, K. E.; Dai, H. J. Electrical and Thermal Transport in Metallic Single-Wall Carbon Nanotubes on Insulating Substrates. *J. Appl. Phys.* **2007**, *101*, No. Art. No. 093710.
6. Coleman, J. N.; Blau, W. J.; Dalton, A. B.; Munoz, E.; Collins, S.; Kim, B. G.; Razal, J.; Selvidge, M.; Vieiro, G.; Baughman, R. H. Improving the Mechanical Properties of Single-Walled Carbon Nanotube Sheets by Intercalation of Polymeric Adhesives. *Appl. Phys. Lett.* **2003**, *82*, 1682–1684.
7. Spitalsky, Z.; Tasis, D.; Papagelis, K.; Galiotis, C. Carbon Nanotube-Polymer Composites: Chemistry, Processing, Mechanical and Electrical Properties. *Prog. Polym. Sci.* **2010**, *35*, 357–401.
8. Miaudet, P.; Badaire, S.; Maugey, M.; Derre, A.; Pichot, V.; Launois, P.; Poulin, P.; Zakri, C. Hot-Drawing of Single and Multiwall Carbon Nanotube Fibers for High Toughness and Alignment. *Nano Lett.* **2005**, *5*, 2212–2215.
9. Kumar, S.; Dang, T. D.; Arnold, F. E.; Bhattacharyya, A. R.; Min, B. G.; Zhang, X. F.; Vaia, R. A.; Park, C.; Adams, W. W.; Hauge, R. H.; et al. Synthesis, Structure, and Properties of PBO/SWNT Composites. *Macromolecules* **2002**, *35*, 9039–9043.
10. Li, Y. J.; Shimizu, H. Toward a Stretchable, Elastic, and Electrically Conductive Nanocomposite: Morphology and Properties of Poly[styrene-*b*-(ethylene-*co*-butylene)-*b*-styrene]/Multiwalled Carbon Nanotube Composites Fabricated by High-Shear Processing. *Macromolecules* **2009**, *42*, 2587–2593.
11. Hwang, G. L.; Shieh, Y. T.; Hwang, K. C. Efficient Load Transfer to Polymer-Grafted Multiwalled Carbon Nanotubes in Polymer Composites. *Adv. Funct. Mater.* **2004**, *14*, 487–491.
12. Shaffer, M. S. P.; Windle, A. H. Fabrication and Characterization of Carbon Nanotube/Poly(vinyl alcohol) Composites. *Adv. Mater.* **1999**, *11*, 937–941.
13. Cadek, M.; Coleman, J. N.; Barron, V.; Hedicke, K.; Blau, W. J. Morphological and Mechanical Properties of Carbon-Nanotube-Reinforced Semicrystalline and Amorphous Polymer Composites. *Appl. Phys. Lett.* **2002**, *81*, 5123–5125.
14. Velasco-Santos, C.; Martinez-Hernandez, A. L.; Fisher, F. T.; Ruoff, R.; Castano, V. M. Improvement of Thermal and Mechanical Properties of Carbon Nanotube Composites through Chemical Functionalization. *Chem. Mater.* **2003**, *15*, 4470–4475.
15. Zhang, X. F.; Liu, T.; Sreekumar, T. V.; Kumar, S.; Hu, X. D.; Smith, K. Gel Spinning of PVA/SWNT Composite Fiber. *Polymer* **2004**, *45*, 8801–8807.
16. Zhang, X. F.; Liu, T.; Sreekumar, T. V.; Kumar, S.; Moore, V. C.; Hauge, R. H.; Smalley, R. E. Poly(vinyl alcohol)/SWNT Composite Film. *Nano Lett.* **2003**, *3*, 1285–1288.
17. Gao, J. B.; Zhao, B.; Itkis, M. E.; Bekyarova, E.; Hu, H.; Kranak, V.; Yu, A. P.; Haddon, R. C. Chemical Engineering of the Single-Walled Carbon Nanotube-Nylon 6 Interface. *J. Am. Chem. Soc.* **2006**, *128*, 7492–7496.
18. Park, S.; Yoon, S. W.; Choi, H.; Lee, J. S.; Cho, W. K.; Kitn, J.; Park, H. J.; Yun, W. S.; Choi, C. H.; Do, Y.; et al. Pristine Multiwalled Carbon Nanotube/Polyethylene Nanocomposites by Immobilized Catalysts. *Chem. Mater.* **2008**, *20*, 4588–4594.
19. Biette, L.; Carn, F.; Maugey, M.; Achard, M. F.; Maquet, T.; Steunou, N.; Livage, T.; Serier, H.; Backov, R. Macroscopic Fibers of Oriented Vanadium Oxide Ribbons and Their Application as Highly Sensitive Alcohol Microsensors. *Adv. Mater.* **2005**, *17*, 2970–2974.
20. Ma, W. J.; Song, L.; Yang, R.; Zhang, T. H.; Zhao, Y. C.; Sun, L. F.; Ren, Y.; Liu, D. F.; Liu, L. F.; Shen, J.; et al. Directly Synthesized Strong, Highly Conducting, Transparent Single-Walled Carbon Nanotube Films. *Nano Lett.* **2007**, *7*, 2307–2311.
21. Chang, C. M.; Liu, Y. L. Functionalization of Multi-Walled Carbon Nanotubes with Non-Reactive Polymers through an Ozone-Mediated Process for the Preparation of a Wide Range of High Performance Polymer/Carbon Nanotube Composites. *Carbon* **2010**, *48*, 1289–1297.
22. Dalton, A. B.; Collins, S.; Munoz, E.; Razal, J. M.; Ebron, V. H.; Ferraris, J. P.; Coleman, J. N.; Kim, B. G.; Baughman, R. H. Super-Tough Carbon-Nanotube Fibres—These Extraordinary Composite Fibres Can Be Woven into Electronic Textiles. *Nature* **2003**, *423*, 703–703.
23. Zhang, M.; Fang, S. L.; Zakhidov, A. A.; Lee, S. B.; Aliev, A. E.; Williams, C. D.; Atkinson, K. R.; Baughman, R. H. Strong, Transparent, Multifunctional, Carbon Nanotube Sheets. *Science* **2005**, *309*, 1215–1219.
24. Sahoo, N. G.; Cheng, H. K. F.; Cai, J. W.; Li, L.; Chan, S. H.; Zhao, J. H.; Yu, S. Z. Improvement of Mechanical and Thermal Properties of Carbon Nanotube Composites through Nanotube Functionalization and Processing Methods. *Mater. Chem. Phys.* **2009**, *117*, 313–320.
25. Vigolo, B.; Penicaud, A.; Coulon, C.; Sauder, C.; Pailler, R.; Journet, C.; Bernier, P.; Poulin, P. Macroscopic Fibers and Ribbons of Oriented Carbon Nanotubes. *Science* **2000**, *290*, 1331–1334.
26. Pei, X. W.; Liu, W. M.; Hao, J. C. Functionalization of Multiwalled Carbon Nanotube *via* Surface Reversible Addition Fragmentation Chain Transfer Polymerization and as

Lubricant Additives. *J. Polym. Sci., Polym. Chem.* **2008**, *46*, 3014–3023.
27. Choi, T. Y.; Poulikakos, D.; Tharian, J.; Sennhauser, U. Measurement of Thermal Conductivity of Individual Multiwalled Carbon Nanotubes by the 3-Omega Method. *Appl. Phys. Lett.* **2005**, *87*, Art. No. 013108.
28. Yang, K.; Gu, M. Y.; Guo, Y. P.; Pan, X. F.; Mu, G. H. Effects of Carbon Nanotube Functionalization on the Mechanical and Thermal Properties of Epoxy Composites. *Carbon* **2009**, *47*, 1723–1737.
29. Ebbesen, T. W.; Lezec, H. J.; Hiura, H.; Bennett, J. W.; Ghaemi, H. F.; Thio, T. Electrical Conductivity of Individual Carbon Nanotubes. *Nature* **1996**, *382*, 54–56.
30. Lu, W. B.; Zu, M.; Byun, J. H.; Kim, B. S.; Chou, T. W. State of the Art of Carbon Nanotube Fibers: Opportunities and Challenges. *Adv. Mater.* **2012**, *24*, 1805–1833.
31. Naraghi, M.; Filleter, T.; Moravsky, A.; Locascio, M.; Loutfy, R. O.; Espinosa, H. D. A Multiscale Study of High Performance Double-Walled Nanotube-Polymer Fibers. *ACS Nano* **2010**, *4*, 6463–6476.
32. Koval'chuk, A. A.; Shchegolikhin, A. N.; Shevchenko, V. G.; Nedorezova, P. M.; Klyamkina, A. N.; Aladyshev, A. M. Synthesis and Properties of Polypropylene/Multiwall Carbon Nanotube Composites. *Macromolecules* **2008**, *41*, 3149–3156.
33. Cao, X. D.; Dong, H.; Li, C. M.; Lucia, L. A. The Enhanced Mechanical Properties of a Covalently Bound Chitosan-Multiwalled Carbon Nanotube Nanocomposite. *J. Appl. Polym. Sci.* **2009**, *113*, 466–472.
34. Wang, W.; Ciselli, P.; Kuznetsov, E.; Peijs, T.; Barber, A. H. Effective Reinforcement in Carbon Nanotube—Polymer Composites. *Philos. Trans. R. Soc., A* **2008**, *366*, 1613–1626.
35. Buehler, M. J.; Ackbarow, T. Fracture Mechanics of Protein Materials. *Mater. Today* **2007**, *10*, 46–58.
36. Tarakanova, A.; Buehler, M. J. A Materiomics Approach to Spider Silk: Protein Molecules to Webs. *JOM* **2012**, *64*, 214–225.
37. Compton, O. C.; Cranford, S. W.; Putz, K. W.; An, Z.; Brinson, L. C.; Buehler, M. J.; Nguyen, S. T. Tuning the Mechanical Properties of Graphene Oxide Paper and Its Associated Polymer Nanocomposites by Controlling Cooperative Intersheet Hydrogen Bonding. *ACS Nano* **2012**, *6*, 2008–2019.
38. Keten, S.; Xu, Z. P.; Ihle, B.; Buehler, M. J. Nanoconfinement Controls Stiffness, Strength and Mechanical Toughness of Beta-Sheet Crystals in Silk. *Nat. Mater.* **2010**, *9*, 359–367.
39. Keten, S.; Buehler, M. J. Geometric Confinement Governs the Rupture Strength of H-Bond Assemblies at a Critical Length Scale. *Nano Lett* **2008**, *8*, 743–748.
40. Filleter, T.; Yockel, S.; Naraghi, M.; Paci, J. T.; Compton, O. C.; Mayes, M. L.; Nguyen, S. T.; Schatz, G. C.; Espinosa, H. D. Experimental-Computational Study of Shear Interactions within Double-Walled Carbon Nanotube Bundles. *Nano Lett.* **2012**, *12*, 732–742.
41. Datsyuk, V.; Kalyva, M.; Papagelis, K.; Parthenios, J.; Tasis, D.; Siokou, A.; Kallitsis, I.; Galiotis, C. Chemical Oxidation of Multiwalled Carbon Nanotubes. *Carbon* **2008**, *46*, 833–840.
42. Liu, K.; Sun, Y. H.; Lin, X. Y.; Zhou, R. F.; Wang, J. P.; Fan, S. S.; Jiang, K. L. Scratch-Resistant, Highly Conductive, and High-Strength Carbon Nanotube-Based Composite Yarns. *ACS Nano* **2010**, *4*, 5827–5834.
43. Ma, W. J.; Song, L.; Yang, R.; Zhang, T. H.; Zhao, Y. C.; Sun, L. F.; Ren, Y.; Liu, D. F.; Liu, L. F.; Shen, J.; et al. Directly Synthesized Strong, Highly Conducting, Transparent Single-Walled Carbon Nanotube Films. *Nano Lett.* **2007**, *7*, 2307–2311.
44. Vilatela, J. J.; Windle, A. H. Yarn-Like Carbon Nanotube Fibers. *Adv. Mater.* **2010**, *22*, 4959–4963.
45. Wu, A. S.; Nie, X.; Hudspeth, M. C.; Chen, W. N. W.; Chou, T. W.; Lashmore, D. S.; Schauer, M. W.; Tolle, E.; Rioux, J. Strain Rate-Dependent Tensile Properties and Dynamic Electromechanical Response of Carbon Nanotube Fibers. *Carbon* **2012**, *50*, 3876–3881.
46. Wu, A. S.; Chou, T. W. Carbon Nanotube Fibers for Advanced Composites. *Mater. Today* **2012**, *15*, 302–310.
47. Li, Y.-L.; Kinloch, I. A.; Windle, A. H. Direct Spinning of Carbon Nanotube Fibers from Chemical Vapor Deposition Synthesis. *Science* **2004**, *304*, 276–278.
48. Zhu, H. W.; Xu, C. L.; Wu, D. H.; Wei, B. Q.; Vajtai, R.; Ajayan, P. M. Direct Synthesis of Long Single-Walled Carbon Nanotube Strands. *Science* **2002**, *296*, 884–6.
49. Zhou, W.; Vavro, J.; Guthy, C.; Winey, K. I.; Fischer, J. E.; Ericson, L. M.; Ramesh, S.; Saini, R.; Davis, V. A.; Kittrell, C.; et al. Single Wall Carbon Nanotube Fibers Extruded from Super-Acid Suspensions: Preferred Orientation, Electrical, and Thermal Transport. *J. Appl. Phys.* **2004**, *95*, 649–655.
50. Davis, V. A.; Pasquali, M. Macroscopic Fibers of Single-Wall Carbon Nanotubes. In *Nanoengineering of Structural, Functional and Smart Materials*; Schulz, M., Kelkar, A., Sundaresan, M., Eds.; CRC Press: Boca Raton, FL, 2004.
51. Gates, T. S.; Jefferson, G. D.; Frankland, S. J. V. Elastic Respoonse and Failure Studies of Multi-Wall Carbon Nanotube Twisted Yarns. *Proceeding of American Society for Composites—Twenty-Second Technical Conference*, Seattle, WA, **2007**.
52. Ryan, K. P.; Cadek, M.; Nicolosi, V.; Blond, D.; Ruether, M.; Armstrong, G.; Swan, H.; Fonseca, A.; Nagy, J. B.; Maser, W. K.; et al. Carbon Nanotubes for Reinforcement of Plastics? A Case Study with Poly(vinyl alcohol). *Compos. Sci. Technol.* **2007**, *67*, 1640–1649.
53. Coleman, J. N.; Cadek, M.; Blake, R.; Nicolosi, V.; Ryan, K. P.; Belton, C.; Fonseca, A.; Nagy, J. B.; Gun'ko, Y. K.; Blau, W. J. High-Performance Nanotube-Reinforced Plastics: Understanding the Mechanism of Strength Increase. *Adv. Funct. Mater.* **2004**, *14*, 791–798.
54. Rath, J. P.; Chaki, T. K.; Khastgir, D. Change in Fiber Properties Due to the Heat Treatment of Nylon 6 Tire Cords. *J. Appl. Polym. Sci.* **2008**, *108*, 3960–3967.
55. Vollrath, F.; Knight, D. P. Liquid Crystalline Spinning of Spider Silk. *Nature* **2001**, *410*, 541–548.
56. Chand, S. Carbon Fibers for Composites. *J. Mater. Sci.* **2000**, *35*, 1303–13.
57. Andrews, R.; Jacques, D.; Minot, M.; Rantell, T. Fabrication of Carbon Multiwall Nanotube/Polymer Composites by Shear Mixing. *Macromol. Mater. Eng.* **2002**, *287*, 395–403.
58. Olek, M.; Ostrander, J.; Jurga, S.; Mohwald, H.; Kotov, N.; Kempa, K.; Giersig, M. Layer-by-Layer Assembled Composites from Multiwall Carbon Nanotubes with Different Morphologies. *Nano Lett.* **2004**, *4*, 1889–1895.
59. Mamedov, A. A.; Kotov, N. A.; Prato, M.; Guldi, D. M.; Wicksted, J. P.; Hirsch, A. Molecular Design of Strong Single-Wall Carbon Nanotube/Polyelectrolyte Multilayer Composites. *Nat. Mater.* **2002**, *1*, 190–194.
60. Koziol, K.; Vilatela, J.; Moisala, A.; Motta, M.; Cunniff, P.; Sennett, M.; Windle, A. High-Performance Carbon Nanotube Fiber. *Science* **2007**, *318*, 1892–1895.
61. Naraghi, M.; Bratzel, G. H.; Filleter, T.; An, Z.; Wei, X.; Nguyen, S. T.; Buehler, M. J.; Espinosa, H. D. Atomistic Investigation of Load Transfer between Dwnt Bundles "Crosslinked" by Pmma Oligomers. *Adv. Funct. Mater.* **2012**, 10.1002/adfm.201201358.
62. Chenoweth, K.; van Duin, A. C. T.; Goddard, W. A. Reaxff Reactive Force Field for Molecular Dynamics Simulations of Hydrocarbon Oxidation. *J. Phys. Chem. A* **2008**, *112*, 1040–1053.
63. Vilatela, J. J.; Elliott, J. A.; Windle, A. H. A Model for the Strength of Yarn-like Carbon Nanotube Fibers. *ACS Nano* **2011**, *5*, 1921–1927.
64. Motta, M.; Li, Y. L.; Kinloch, I.; Windle, A. Mechanical Properties of Continuously Spun Fibers of Carbon Nanotubes. *Nano Lett.* **2005**, *5*, 1529–1533.
65. Plimpton, S. Fast Parallel Algorithms for Short-Range Molecular Dynamics. *J. Comput. Phys.* **1995**, *117*, 1–19.